Hydrogen absorption kinetics at titanium surfaces as measured using ERDA
by Marcus Alton Teter

A thesis submitted in partial fulfillment of the requirements for the degree of Master of Science in Physics
Montana State University

Abstract:
Since titanium alloys are being studied for aerospace usage, the hydrogen absorption characteristics of the alloys must be known. Using titanium metal as a baseline, elastic recoil detection analysis (ERDA) was chosen to measure the hydrogen concentration profile. ERDA allowed for the measurement of both the surface and bulk concentrations of hydrogen with the same experimental equipment, rather than previous methods which required that the two sets of experimental equipment be calibrated with respect to each other. The results allowed for the determination of surface and bulk concentrations of hydrogen as a function of exposure time. ERDA was concluded as being a useful technique for measuring the hydrogen uptake properties of metals.

HYDROGEN ABSORPTION KINETICS AT TITANIUM SUFACES AS MEASURED USING ERDA

By

Marcus Alton Teter

A thesis submitted in partial fulfillment
of the requirements for the degree

of

Master of Science

in

Physics

MONTANA STATE UNIVERSITY, BOZEMAN
Bozeman, Montana

December 1996

APPROVAL

of a thesis submitted by

Marcus Alton Teter

This thesis has been read by each member of the thesis committee and has been found to be satisfactory regarding content, English usage, format, citations, bibliographic style, and consistency, and is ready for submission to the College of Graduate Studies.

Dr. Richard J. Smith — Richard J. Smith (Signature) — 1-27-97 Date

Approved for the Department of Physics

Dr. John C. Hermanson — (Signature) — 1-27-97 Date

Approved for the College of Graduate Studies

Dr. Robert Brown — (Signature) — 2/3/97 Date

STATEMENT OF PERMISSION TO USE

In presenting this thesis in partial fulfillment of the requirements for a master's degree at Montana State University-Bozeman, I agree that the Library shall make it available to borrowers under rules of the Library.

If I have indicated my intention to copyright this thesis by including a copyright notice page, copying is allowable only for scholarly purposes, consistent with "fair use" as prescribed in the U.S. Copyright Law. Requests for permission for extended quotation from or reproduction of this thesis in whole or in parts may be granted only by the copyright holder.

Signature Mona A. Peters

Date 19 DEC 1996

TABLE OF CONTENTS

LIST OF TABLES

LIST OF FIGURES

ABSTRACT

Since titanium alloys are being studied for aerospace usage, the hydrogen absorption characteristics of the alloys must be known. Using titanium metal as a baseline, elastic recoil detection analysis (ERDA) was chosen to measure the hydrogen concentration profile. ERDA allowed for the measurement of both the surface and bulk concentrations of hydrogen with the same experimental equipment, rather than previous methods which required that the two sets of experimental equipment be calibrated with respect to each other. The results allowed for the determination of surface and bulk concentrations of hydrogen as a function of exposure time. ERDA was concluded as being a useful technique for measuring the hydrogen uptake properties of metals.

1.0 INTRODUCTION

Hydrogen absorption by metals has been an ongoing field of investigation for nearly twenty years. Early investigations focused on hydrogen storage techniques, using the metal as a reservoir for the hydrogen. Later, the investigations were geared toward the problem presented by hydrogen embrittlement of materials, especially those materials intended for aerospace applications.

In the case of the national aerospace plane (NASP), the focus has been upon the embrittlement problem. The aerospace plane was intended to be primarily fueled by hydrogen. The weight and strength of materials focused design efforts toward titanium based alloys. Unfortunately, titanium readily absorbs hydrogen, so understanding the characteristics of the absorption and the resulting embrittlement is essential toward using titanium alloys and other materials. In the extreme conditions of flight, there are expected to be thermal conditions which will take materials from cryogenic temperatures to extremely high temperatures in very rapid succession or leave the material at the extremes for long duration. The flight mechanical characteristics for the material must include the ability to withstand high pressure loads and extreme acoustic loads.[1] Any degrading of the titanium alloys by hydrogen would have disastrous effects.

Hydrogen can degrade materials through a number of interactions. On the surface, the hydrogen can be adsorbed to form a hydride. In the bulk, the hydrogen may move into the material forming bonds that lead to hydrides, dislocate substrate atoms that

reduce the material's structural integrity, or form pockets of hydrogen gas.[1] Consequently, material interactions with hydrogen fall into two categories: (1) surface interactions, and (2) bulk interactions.

The techniques that have been previously used for the study of hydrogen uptake by materials focus on measurement of either of these two areas. The surface adsorption has been measured using photoemission[2]. The bulk uptake has been measured using resistivity techniques[2] and by quartz crystal microbalance (QCM).[3] Both types of experimental techniques are successful in their own right, but to get the entire range of data of both surface and bulk interactions requires that the two types of experiments must be calibrated with respect to each other. Clearly, there should be an advantage to simultaneously measuring both bulk and surface concentrations of hydrogen with one technique.

This work represents a baseline set of experiments to demonstrate an experimental technique that will measure both surface and bulk hydrogen content simultaneously. Elastic recoil detection analysis (ERDA) was used to demonstrate measurements of hydrogen uptake in titanium. The advantage of ERDA is that it can be used to probe deeply into the sample, thus showing concentrations as a function of depth. Subsequently, the kinetics of the uptake interactions can be more easily understood.

Section 2, of this work, describes the experimental apparatus used for the hydrogen exposure experiments. The basic theory of the measurement techniques is detailed in Section 3. A model for data analysis is presented in Section 4. Section 5 presents the experimental results. Lastly, discussion of the results and concluding remarks appear in Section 6.

2. EXPERIMENTAL EQUIPMENT

2.1 UHV Chamber

The UHV (Ultra High Vacuum) Chamber, as pictured in figure 2.1.1, was the primary experimental apparatus. It was connected by way of a differentially pumped beam line to the 2 MV Van de Graaff accelerator. The chamber contained pumping systems capable of vacuum pressures of 10^{-10} Torr after appropriate chamber baking. The UTI mass spectrometer was used for determining relative residual gas concentrations. The sputter gun was used for sample cleaning. The Auger spectrometer determined the surface characteristics. Also, two detectors were used for ion beam measurements. The gas system provided either argon gas for sample cleaning, or hydrogen gas for exposure experiments. The sample location within the chamber was controlled by a Varian 3 axis-goniometer, attached to a sample holder specifically designed for holding thick metal samples.

The pumping apparatus dominated the vacuum system. A mechanical roughing pump brought the chamber pressure down to tens of microns of Hg. A turbo pump, placed in line with the roughing pump, provided pressures down to 10^{-7} Torr prior to baking; furthermore, it provided a method of keeping gas cycling in the chamber during sample cleaning and hydrogen exposure. The ion pump allowed pressures to 10^{-9} Torr, after chamber baking. A gate valve, closed during argon and hydrogen exposures,

prevented ion pump contamination during hydrogen exposure. Lastly, titanium sublimation provided pumping since titanium adsorbed gasses such as hydrogen; appropriate deposition of titanium on chamber walls provided means to attain 10^{-10} Torr.

The UTI mass spectrometer allowed for the determination of the components of residual gas in the chamber. It was useful for determining the source of a leak. For example, when one of the leak valves was not properly closed, argon gas was present in the chamber preventing pressures from reaching 10^{-10} Torr. Using the UTI helped isolate the source of the leak, which led to quick corrective measures. The UTI was also used to verify the purity of the gas sources. For instance, if either the argon or the hydrogen gas were contaminated with water, introduction of the gas in the chamber would defeat the efforts of baking.

Once UHV had been achieved, contaminants were present on the sample in the form of organic material and oxides. These materials needed to be removed from the sample surface so that the surface characteristics would be well defined. All the contaminants previously mentioned could be removed by heating to temperatures higher than 600°C; however, at these temperatures, sulfur would diffuse out of the bulk of the sample onto the surface. Such a situation left undesirable surface conditions, so the sulfur had to be removed. Removal could have been accomplished by heating the sample to the sulfur sublimation point, but, since a titanium phase change exists at a lower temperature, excessive heating was avoided. The removal of sulfur was accomplished using a 2kV sputter gun, which ionized argon gas and accelerated it toward the sample surface, knocking off the surface contaminants as a result of collision. Since the sulfur did not

bind tightly to the surface, one hour of sputtering at a microampere per square centimeter of sample current was sufficient to remove sulfur.

The characteristics of the sample surface were determined by Auger Electron Spectroscopy (AES). Section 3.1 details the theory of AES. Surface characteristics could have been determined throughout the exposure series, but in the interest of maximizing usable concentration data, the AES measurements were confined to the beginning and the end of an exposure series. Once surface characteristics were sufficiently determined to begin an exposure, the AES electronics were shut off to avoid noise in the solid state detectors used for the ion beam experiments.

Two solid state detectors were present in the chamber. The first used a rotating axis, providing the ability to detect reflected particles at any azimuthal direction. It was typically fixed at a scattering angle of 155 degrees, the best possible angle for Rutherford Back Scattering that determined the incident beam energy (see Section 3.2). The second detector used a fixed mount at a scattering angle of 25 degrees, representing a good scattering angle for the forward scattering technique of ERDA, detailed in Section 3.2.

A two-line gas system allowed for the separate use of two different gases, eliminating the possibility of contamination of one gas line with differing gases. Each gas line had its own shut-off valve, regulator, and leak valve; both lines had valves which could be opened for pumping the lines clean with the turbo pump. Periodically, the lines were evacuated and heated to insure contaminant-free gasses. When not in use, the lines typically had higher than atmospheric pressure of gas to prevent atmospheric contaminant gases from entering the system.

Attached to a Varian 3-axis goniometer, a new sample holder was built to handle thick, approximately 1 millimeter, samples (see Figure 2.1.2). Heating the sample was accomplished by electron beam heating, where the sample was put at a high potential and the filament generated thermionic electrons. Careful control of the filament current allowed very precise control of the sample temperature, which was measured using a thermocouple attached to the rear surface of the sample. Temperatures were kept below 750°C to avoid a phase transition of the titanium samples.

Overall, the UHV chamber allowed precise control of experimental conditions, minimizing contaminants. Once ultra-high vacuum conditions were established, hydrogen uptake experiments could be performed using a variety of surface conditions; consequently, UHV became essential to measure any significant uptake.

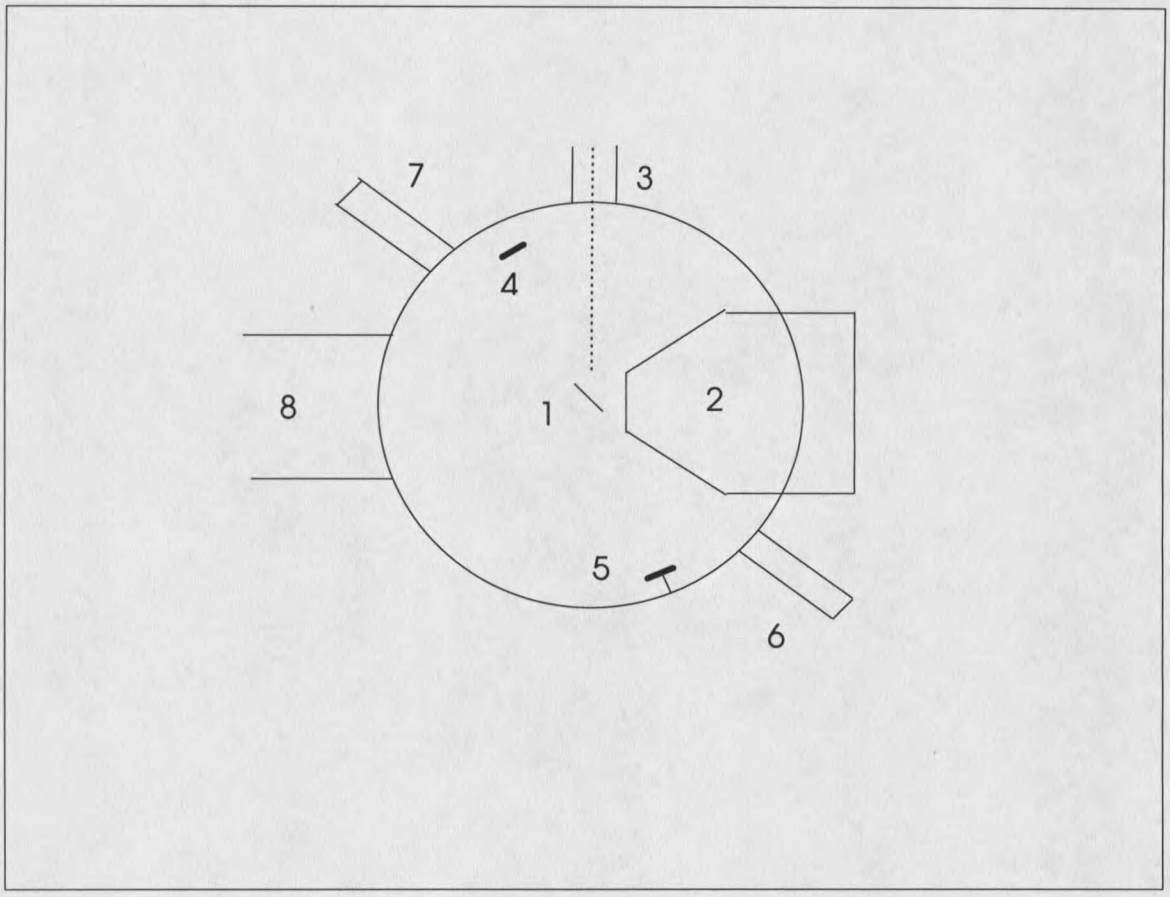

Figure 2.1.1

Schematic of UHV chamber.

(1) The sample, (2) the Auger cylindrical mirror analyzer, (3) ion beam path from accelerator, (4) movable solid state detector for RBS, (5) fixed solid state detector for ERDA, (6) gas system, (7) UTI mass spectrometer, (8) connection to pumps.

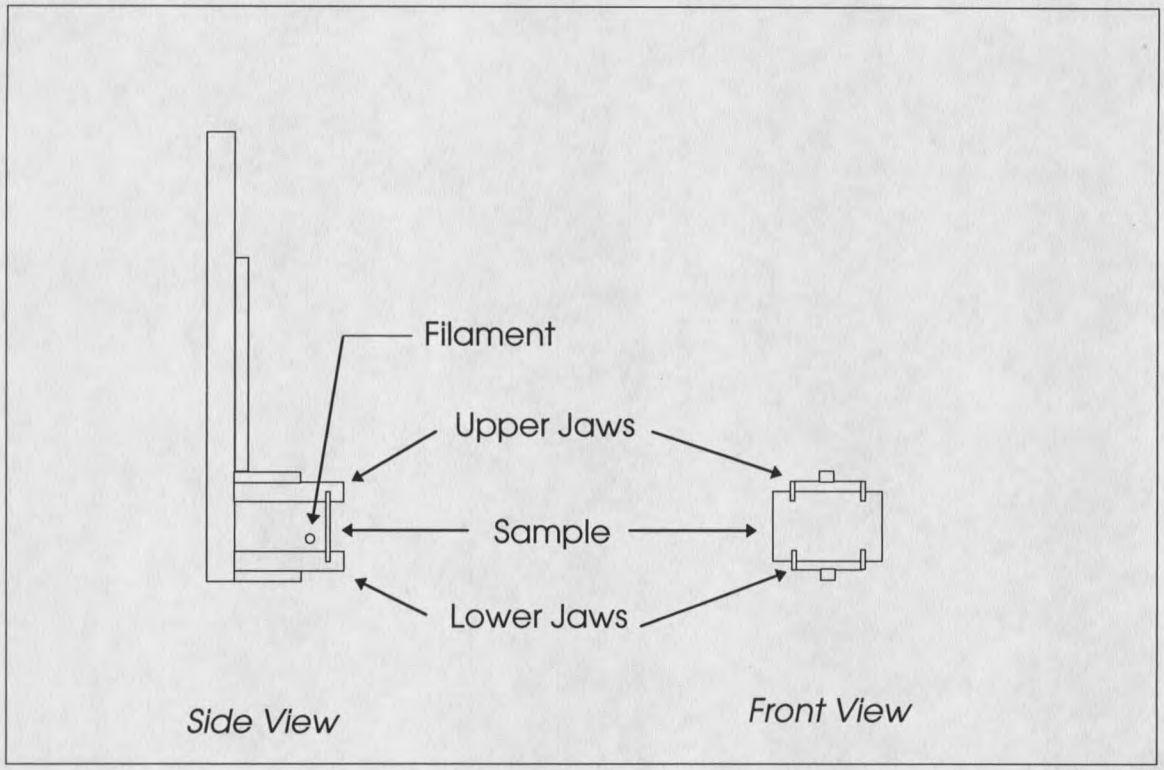

Figure 2.1.2

Schematic of sample holder designed for thick, approximately 1mm, samples. Note that sample heating is accomplished by electron beam heating. The jaws are made of tantalum. The frame is made of aluminum.

2.2 The Van de Graaff Accelerator

The Van de Graaff accelerator provided a source of alpha particles (helium ions) which were used for the ion beam techniques detailed in Section 3.2. The Van de Graaff operates on the principle of static charge separation, where one end of the accelerator is positively charged, the source end. Positive ions were created at the source end, forcing them to accelerate away from the positively charged end. The ions, once leaving the front of the accelerator, entered a bending magnet that allowed ions to be separated by kinetic energy. The magnetic field could be controlled to specifically bring the singly ionized helium down the beam line to the UHV chamber and sample.

Setting up the high potential was accomplished by a belt transporting electrons away from the terminal end of the accelerator apparatus. A simplified picture of a typical Van de Graaff generator (see Figure 2.2.1) proved useful for understanding the principle of operation. The belt was set into rapid rotation. The positively charged source point removed electrons from the belt which in turn removed electrons from the metal dome. Moving electrons to the front of the accelerator, in this manor, allowed for a very large potential difference to exist. Though some accelerators have potentials up to 20 million volts, this Van de Graaff was limited to a potential of 1.9 million volts. A controlled discharge, known as corona discharge, near the dome (not shown) allowed for precise control of accelerator voltage.

If an ionized particle, with charge Ze, was introduced in the interior of the charged

dome, it would move along the electric field generated by the large potential difference. The resulting particle had kinetic energy

$$E_0 = Ze\Delta\phi \tag{2.2.1}$$

at the end of the accelerator. By allowing the ion to pass through the end of the accelerator, a usable source of ions at a kinetic energy as specified by equation 2.2.1 was available.

Unfortunately, because of ionization of residual gases along the acceleration column, many accelerated species were present at the front with varying kinetic energies based upon their level of ionization. Singling out a specific ion species at a particular kinetic energy was accomplished with a bending magnet. Any charged particle that enters a magnetic field with a momentum $p_\perp=(2mE_0)^{1/2}$, perpendicular to the field, will move in a circular path of radius

$$r = \frac{cp_\perp}{|Z|eH} \tag{2.2.2}$$

where H represents the magnetic field strength, determined by current flowing through the magnet coils. Thus, the desired particle of charge Ze and mass m could be delivered down the beam line at the desired energy, E_0.

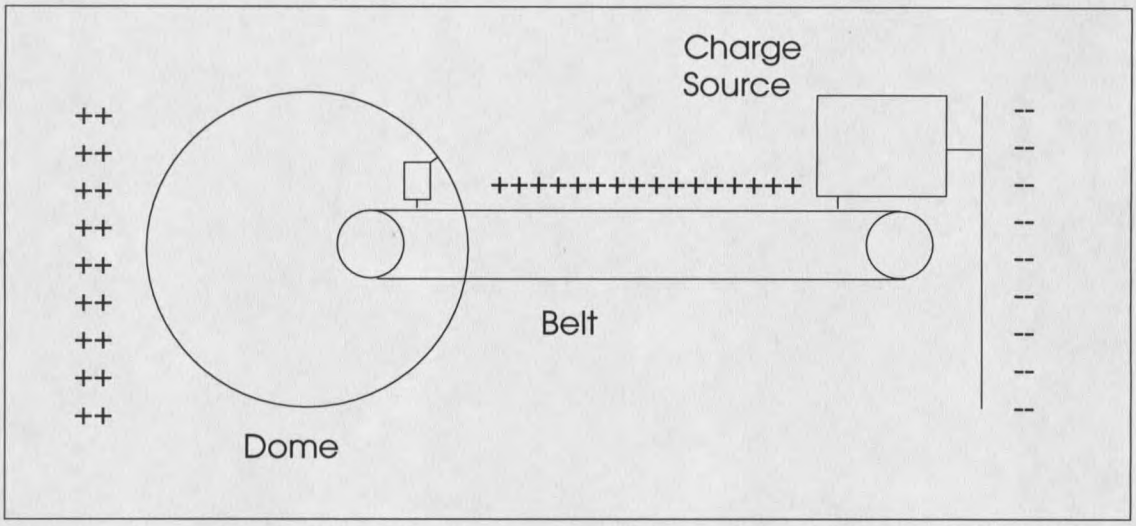

Figure 2.2.1

Schematic diagram of Van de Graaff Generator.

Note that the charge source strips electrons from the belt thereby giving a net positive charge at the dome or terminal end. A beam line may be placed along the axis of the generator, allowing positively charged ions to be accelerated out the front end.

3. THEORY OF EXPERIMENTAL TECHNIQUES

3.1 AES

Auger Electron Spectroscopy (AES), was used to determine the characteristics of the metal surface with respect to the presence and relative concentrations of contaminants. The Auger process is the particle counterpart of fluorescence, since multiple electron atoms can drop an electron down to a lower energy state by freeing another electron instead of emitting a photon. In fact, the Auger decay occurs with higher probability than fluorescence as the number of electrons increases. Thus, the Auger process became a fundamental quantum mechanical process.

Typically, the AES apparatus and data acquisition was straightforward. An election gun ionized the atom, leaving an unoccupied energy state. An analyzer detected the released Auger electron and measured its energy. The analyzer, used for the equipment detailed in Section 2.1, was a cylindrical mirror analyzer (CMA). The CMA operated by selecting an energy for detection and would give a signal based upon the number of electrons incident upon it. By changing the potential on the outer cylinder of the CMA, electrons of corresponding energies were passed to the detector, resulting in an Auger spectrum of intensity as a function of energy [for details of the AES apparatus reference Schaus and Smith[4] or the AES manual[5]].

The basic principles governing the Auger process require that a single electron bound state of an atom be empty. The empty state could be created by any number of

processes, but a common method is by knocking the electron out of the atom by another high energy electron. Once the electron had been knocked out of the atom, there remains a vacancy at the energy level, leaving the atom in an exited energy state (see Figure 3.1.1a). The atom can return to a lower energy state by dropping an electron to the empty state. However, quantum mechanical conservation laws demand that the energy lost by the decaying electron must be gained by another particle. Fluorescence conserves the energy by creation of a photon, but Auger emission conserves the energy by transferring it to another electron, thereby raising it to an even more exited state or freeing it from the atom (see Figure 3.1.1b).

Since the energy states for an element were characteristic to each element, the Auger electrons will be characteristic to the element emitting the electron. The characteristic Auger energies, as presented in Table 3.1.1, depend upon the electron shell of all three electrons involved in the process. Consequently, the KLL Auger process signified an empty K shell being filled by an L shell electron causing the liberation of another L shell electron.

AES energies could be specified by an empirical expression:

$$E_{Z,abc} = E_{Z,a} - E_{Z,b} - E_{Z,c} - \frac{1}{2}[E_{Z+1,c} - E_{Z,c} + E_{Z+1,b} - E_{Z,b}] \tag{3.1.1}$$

with Z representing the atomic number and a, b, and c describing the process, such as KLL.[4] Unfortunately, there exists no analytical formula which gives the resulting Auger energies, since the quantum mechanical representation of the matrix element for multiple electron interactions within an atom requires an analytic representation of a multiple

electron atom that has not been done to date.

Once an Auger spectrum had been taken, the relative intensities of the spectral lines corresponding to the individual elements could be compared to find relative concentrations of those elements on the surface. The relative concentration of an element, defined by

$$C_z = \frac{I_z / S_z}{\sum_j I_j / S_j} \tag{3.1.2}$$

with I being the intensity of a spectral line and S being the sensitivity factor of the same line (see Table 3.1.2 for sensitivity factors of interest), determined the characteristics of a surface.

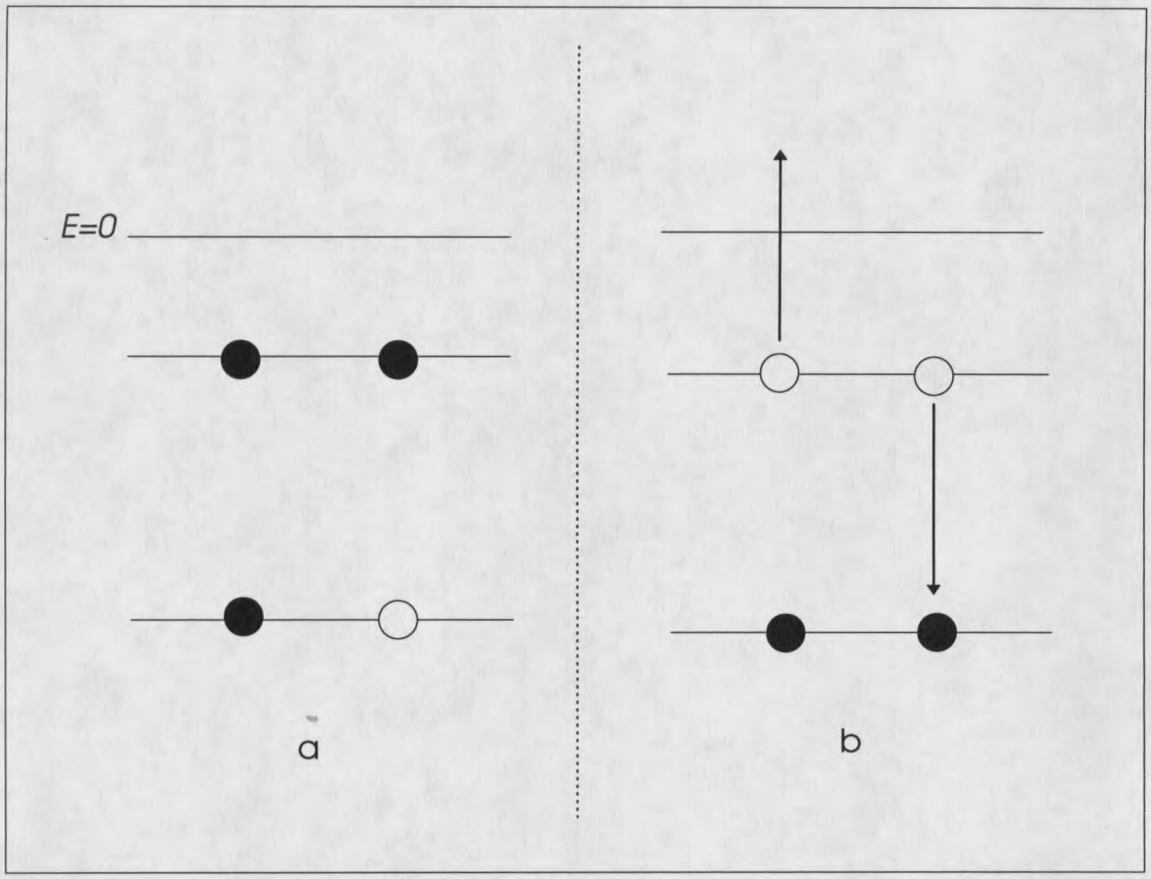

Figure 3.1.1

The Auger Process.

Atom in excited energy state (a) will decay to a less excited state (b) by emitting an electron. Conservation of energy requires that the emitted electron's energy be increased by the amount of energy lost by the decaying electron. Measurement of the energies of Auger electrons will provide a signature of the element which emitted the electron.

Element and Auger Transition Process	Auger Energy (eV)
Titanium, MNN, LMM, LMM	40, 390, 410
Carbon, KLL	270
Oxygen, KLL	510
Sulfur, LMM	150

Table 3.1.1

Auger energies for selected elements and transition processes.[5]

Element and Transition Process	Sensitivity factor
Titanium, LMM	.45
Sulfur, LMM	.8
Carbon, KLL	.16
Oxygen, KLL	.5

Table 3.1.2

Auger sensitivity factors for selected elements and transition processes.[4]

3.2 ERDA

Elastic Recoil Detection Analysis (ERDA), also known as Forward Recoil Spectroscopy (FRS), is a method by which the concentration of an element within a sample may be measured by bombarding the sample with a heavier element of known kinetic energy. For detection of hydrogen in metals, the obvious choice for the heavier element is helium. The collisions involved in ERDA are between charged nuclei, so the cross sections are on the order of 1 barn, 10^{-24} cm^2. Collisions with the electrons present in the sample occur, but the energy and momentum lost in each interaction is small allowing all such interactions to be represented by a stopping rate, energy loss per unit length, for the material that the ion passes. A careful analysis of the collision of the nuclei, using classical physics, leads to a good overview of theoretical considerations involved in ERDA.

Analysis of a classical collision, see Figure 3.2.1 , gives the characteristics necessary for determining parameters to interpret an ERDA spectrum. The collision is considered a completely elastic event between the nuclei of the participant atoms, ignoring the effects of electrons in the interaction. The equations for evaluating the kinematics of the collision are

$$E_0 + E_1 = E_2 + E_3, \tag{3.2.1}$$

from conservation of energy, and the two equations,

$$\left(2m_0E_0\right)^{1/2} + \left(2m_1E_1\right)^{1/2} = \left(2m_2E_2\right)^{1/2}\cos\theta_2 + \left(2m_3E_3\right)^{1/2}\cos\theta_3 \tag{3.2.2}$$

and

$$(2m_2E_2)^{1/2}\sin\theta_2+(2m_3E_3)^{1/2}\sin\theta_3=0, \qquad (3.2.3)$$

from conservation of linear momentum. By fixing θ_2 as the known scattering angle, and noting that the kinetic energy of the target, E_1, is zero, the above equations may be solved for the energy of the particle moving along the known scattering angle, where a detector may be located. So the energy at the detector is given by

$$E_2=\frac{\left[(m_3-m_0)(m_3+m_2)+2m_0m_2\cos^2\theta_2\right]E_0}{(m_3+m_2)^2} \pm\frac{\left[m_0m_2(m_3-m_0)(m_3+m_2)+m_0^2m_2^2\cos^2\theta_2\right]^{1/2}2E_0\cos\theta_2}{(m_3+m_2)^2}. \qquad (3.2.4)$$

Assuming that there is no mass transfer in the collision, which is reasonable for a classical collision involving atomic nuclei, the masses m_2 and m_3 are either m_0 of the incident particle, or m_1 of the target particle.

There are two important cases for equation 3.2.4. If $m_3=m_1$, then the energy of the incident helium nuclei can be determined by elastically scattering it off the metal nuclei through a large angle θ_2. Also, the first case determines the energy of forward scattered helium, by small θ_2, when colliding with the metal nuclei. Secondly, if $m_3=m_0$, then the energy of the forward scattered hydrogen nuclei can be determined from equation 3.2.4.

In the first case, where $m_3=m_1=M$ (M being the mass of the metal nuclei) and $m_2=m_0$, equation 3.2.4 reduces to

$$E_2 = \left[\frac{\left(M^2 - m_0^2 \sin^2 \theta_2\right)^{1/2} + m_0 \cos\theta_2}{m_0 + M} \right]^2 E_0 \qquad (3.2.5)$$

where the quantity multiplying E_0 is the kinematic factor, κ, for Rutherford Back-scattering Spectroscopy (RBS).[6] RBS is the method used to determine the incident energy of the helium beam. Using the mass of the metal nuclei making up the sample, M, and the mass of incident helium nuclei, m_0, RBS allows determination of the incident energy through the relation

$$E_0 = E_2 / \kappa \qquad (3.2.6)$$

Figure 3.2.2 shows a typical RBS spectrum. The forward edge of the spectrum (a) represents the classically scattered helium atom leaving the surface of the material. Typically, RBS was done at a scattering angle, $\theta_2 = 155^o$, giving a kinematic factor of $\kappa = 0.7172$ for a titanium sample.

Furthermore, the first case allows determination of the forward scattered helium energy at angle $\theta_2 = 25^o$ with respect to the detector. Subsequently, the helium atom which scatters elastically off the titanium surface has energy, $E_2 = 0.9848E_0$, creating a problem that will be specified below.

The second case, where $m_3 = m_0$ and $m_2 = m_1$ (m_1 being the mass of the forward scattered hydrogen atom), reduces equation 3.2.4 to

$$E_2 = \left[\frac{4m_0 m_1 \cos^2 \theta_2}{\left(m_0 + m_1\right)^2} \right] E_0 \qquad (3.2.7)$$

where the quantity in square brackets is the kinematic factor, k, for ERDA. Note that the squared cosine makes the best angles of choice to be small. The scattering angle will be further optimized for the scattering cross-section, as shown below.

By comparison, the energy of a scattered helium atom at the detector, as detailed above at $\theta_2 = 25^o$, is $E_{He} = 0.9848E_0$ and the energy of the hydrogen atom forward scattered to the detector, given by equation 3.2.7 at the same angle, is $E_H = 0.5257E_0$. Clearly, the classical scattering event would be adequate for distinguishing hydrogen from helium, based upon the particle energies, but in both cases, the energy measured at the detector is decreased depending upon the depth of the scattering event within the material. The scattered nuclei will lose energy from the multiple collisions with electrons in the material. Unfortunately, this will cause the spectrum for both hydrogen and helium to be spread from zero energy up to the energy of the surface collision, giving overlapping energy spectra and effectively burying the hydrogen spectrum within the helium spectrum.

Using the knowledge of the stopping power, it is possible to remove the helium background spectrum from the hydrogen signal. Building a classical model of the multiple scattering interactions has little practical value; experimental data of the energy loss of particles with well defined energies passing through materials are used to provide a best fit function of energy loss known as the stopping power.[7] Figure 3.2.3 shows the stopping powers for hydrogen and helium within aluminum. Note that for higher energies the helium stopping function is greater than that for hydrogen. Consequently, an

aluminum stopper foil of 8 micrometers may be used to stop helium nuclei from reaching the detector. The hydrogen energy is also decreased, but the particle is not stopped by the foil.

Working backward from the detector, since the energy of the hydrogen is measured, the analysis of the ERDA spectra may begin. Analysis begins at the stopper foil (see Figure 3.2.4). The detector measures the energy of the incoming hydrogen nuclei, E_H. The energy for the hydrogen is

$$E_H = E_{OUT} - \Delta E_s(E_{OUT}), \tag{3.2.8}$$

where $\Delta E_s(E_{OUT})$ is the energy loss due to the stopper foil as a function of energy, and E_{OUT} is the energy of hydrogen leaving the sample.

Unfortunately, the stopper foil also decreases the resolution of the energy measurement. Suppose that a collection of protons enter the stopper foil with energy E_{OUT}. The measured energies of the hydrogen nuclei entering the detector will have a distribution of energies. The loss of energy resolution is known as straggling. References[8,9] present a good theoretical development of straggling effects. In essence, the protons moving through the material along different trajectories encounter non-stationary electrons and target nuclei, and through the collision process, the nuclei lose energy depending upon the impact parameters of the collisions. The variance of the energy, straggling, takes the form

$$\delta(\Delta E_S) = 2(2\ln 2)^{1/2} Z_1 e^2 \sqrt{4\pi N Z_2 t}, \tag{3.2.9}$$

where t is the thickness of the foil, and N is the number density of target atoms in the foil.

Now, moving backward along the particle trajectory in Figure 3.2.4, the next item for characterization is the energy of the hydrogen leaving the sample, E_{out}. The energy of the hydrogen leaving the sample has a maximum value defined by the elastic collision occurring at the surface, $E_{MAXout} = 0.5257E_0$. Consequently, the energies associated with hydrogen originating from beneath the surface will depend upon the stopping power of the sample. Since the hydrogen loses energy coming out of the sample, it is reasonable to assume that the incident helium will also lose energy going into the sample. By combining this into a single energy loss term, then

$$E_{OUT} = kE_o - [S]x, \tag{3.2.10}$$

where x is the depth of the collision and $[S]$ is the stopping power associated with the material. The stopping power $[S]$ has two contributions. The first contribution will be the energy lost by the helium nuclei prior to the collision, and the second will be the energy lost by the hydrogen after the collision. So, the stopping power is given by

$$[S] = \frac{kS_1}{\sin\alpha} + \frac{S_2}{\sin(\theta_2 - \alpha)}, \tag{3.2.11}$$

where S_1 is the stopping power of helium in the material and S_2 is the stopping power for hydrogen in the material. By assuming that the energy lost is small, as a first approximation, then the stopping powers can be evaluated at the surface energies. The stopping power of helium may be written as a function

$$S_1 = S_1(E_o), \tag{3.2.12}$$

and the stopping power of hydrogen may be written as a function

$$S_2 = S_2(E_{OUT}). \tag{3.2.13}$$

Again the stopping power for the material adds to the energy resolution error for the system; however, most of the effects are considerably less than that of the stopping foil so for the deepest portion of the sample, 1000 Å, the stopping foil straggling is still an order of magnitude larger than the straggling associated with the sample.

Finally, the energy measured at the detector as a function of depth may be stated as

$$E_H = kE_0 - \Delta E_S - [S]x, \tag{3.2.14}$$

where the kinematic factor, k is defined by equation 3.2.7, the energy loss due to the stopper foil is a tabulated value, and the stopping power of the sample is defined by equation 3.2.12-13. By solving for x, the depth as a function of energy determined at the detector is found.

The solid state detector used for the ERDA experiment registers counts in a particular channel. The counts are the number of incoming hydrogen atoms knocked out of the sample. The yield, number of counts per channel, of hydrogen at the detector is

$$Y = Q\Omega(\rho\delta x)\sigma \tag{3.2.15}$$

where Q is the number of helium atoms hitting the surface (found through charge integration), Ω is the solid angle of the detector, σ is the scattering cross-section for the collision, and $(\rho\delta x)$ is the number of hydrogen atoms per unit area in a slab of thickness,

δx at depth x. Thus equation 3.2.15 may be rewritten as

$$\rho(x)\delta x = \frac{Y}{\Omega Q \sigma}. \tag{3.2.16}$$

Since Y is the yield per channel, $N(E)$ is defined as the yield per keV, and the factor δE is introduced as the energy per channel. The differentials may be grouped together, and their quotient may be defined as some generalized stopping power, being an energy loss per unit length. The generalized stopping power is [S]/0.63 (see Saleh[10] for a detailed derivation), where [S] is the stopping power of the material. The 0.63 comes from the straggling effects of the stopper foil and is dependent upon the thickness and composition of the foil (aluminum foil of 8 μ m in this case). Thus the density of hydrogen within the sample is

$$\rho(x) = \frac{N(E)[S]}{0.63\Omega Q \sigma}. \tag{3.2.17}$$

Together with equation 3.2.14, equation 3.2.17 allows the analysis of an ERDA spectra. A hydrogen concentration versus depth profile may be made. The only issue that needs additional comment is the collision cross-section.

The helium collision with hydrogen may be viewed as classical. Thus as a first approximation the cross-section may be equated to the Rutherford cross-section; however, because helium nuclei kinetic energy, E_0, is in the 1.5-2.0MeV range, the interaction is not strictly classical. At these high energies, the nuclear forces begin to contribute to the cross-section, so it deviates from the classical Rutherford cross-section. Baglin et al.[11] have developed a polynomial expression which closely matches data for the

cross-section at various scattering angles. The polynomial is

$$\ln[\sigma(E,\theta)] = aE + b + cE^{-1} + dE^{-2}, \tag{3.2.18}$$

where the coefficients *a, b, c,* and *d* are functions of the scattering angle. Equation 3.2.18 combined with the appropriate coefficients (see Baglin et al.[11] Table 1) give a scattering cross-section which is up to nearly twice the Rutherford cross-section for the energies of interest. Such a deviation is significant for determining accurate concentrations of hydrogen.

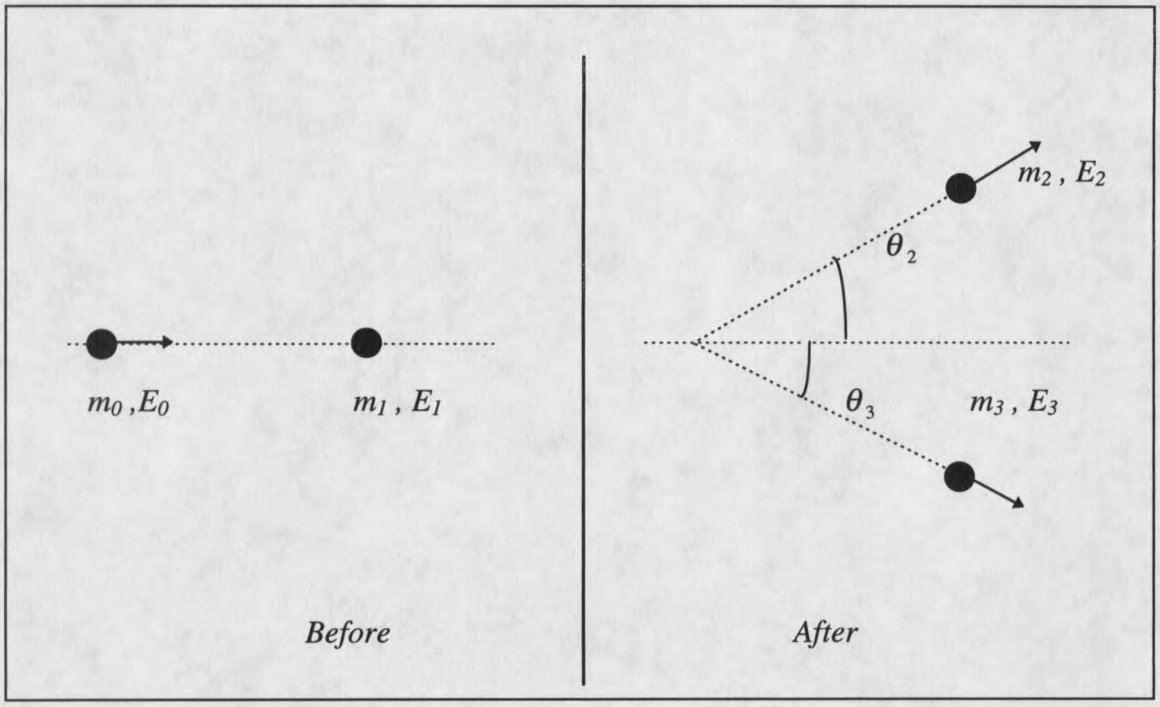

Figure 3.2.1

Classical collision between two point particles..

Note that m_2 can be either m_0 or m_1.